

ANALYSIS OF THE MARTENSITE VARIANT SELECTION IN A SINGLE CRYSTAL CU-AL-BE SHAPE MEMORY ALLOY IN A TENSILE TEST

Fernando Néstor García Castillo

Departamento de Materiales y Manufactura,
DIMEI, Universidad Nacional Autónoma de
México

Ciudad de México, México

<https://orcid.org/0000-0002-0327-1338>

Rafael Schouwenaars

Departamento de Materiales y Manufactura,
DIMEI, Universidad Nacional Autónoma de
México

Ciudad de México, México

Department of Electromechanical, Systems
and Metals Engineering, Ghent University
Belgium

<https://orcid.org/0000-0003-4699-6061>

Jacinto Cortés Pérez

Centro Tecnológico Aragón, FES Aragón,
UNAM
México

Vicente Amigó Borrás

Universitat Politècnica de València, Instituto
de Tecnología de Materiales
Spain

<https://orcid.org/0000-0002-2107-0273>

Miguel Ángel Ramírez Toledo

Departamento de Materiales y Manufactura,
DIMEI, Universidad Nacional Autónoma de
México

Ciudad de México, México

All content in this magazine is licensed under a Creative Commons Attribution License. Attribution-Non-Commercial-Non-Derivatives 4.0 International (CC BY-NC-ND 4.0).



Abstract: This work analyses the crystallographic martensite variants (*MVs*) which are activated in a *Cu-Al-Be* monocrystal subject to a tensile test. Four variants were observed in-situ and analyzed by means of the Schmid Factor (*SF*) criterion. A finite element simulation was performed to obtain the stress in the regions where the martensite variants are observed. The results of the simulation are in good agreement with the variants predicted by the *SF*, with only small deviations from the ideal orientation of the martensite phase. This result provides interesting information to be used in future refinements of the criteria presented in earlier research.

Keywords: Shape memory alloy, martensite, variant selection, monocrystal, tensile test, Schmid factor.

INTRODUCTION

In mechanical engineering applications, shape memory alloys (*SMA*s) are interesting due to effects such as pseudoelasticity and superelasticity as well as the one and two way shape memory effects (Kumar & Lagoudas, 2008; Lexcellent, 2013). Although the shape memory effect is the most famous manifestation of martensitic transformation in metastable alloys, many important applications exploit the pseudoelastic behavior, which is associated with a large recoverable strain (up to 18%) upon loading and unloading (Otsuka, K., & Wayman, 1999). These include wires used as kernel components for seismic protection devices, cellular phone antennas, eyeglass frames, orthodontic devices and thin films in medical devices (Yamauchi et al., 2011; Yoneyama et al., 2010; Zamponi et al., 2009).

Although the phenomenological behavior, geometric laws and thermodynamics of *SMA* single crystals are relatively well understood (Gao et al., 2000; Hall et al., 2007; Huang & Brinson, 1998) many of the current

applications for *SMA*s use polycrystalline alloys, in many occasions with ultrafine grain sizes. Therefore, better mathematical descriptions for such materials are required (Dimitris C. Lagoudas et al., 2006; Lu & Weng, 1998; Martínez-Fuentes et al., 2013; Sánchez & Pulos, 2006). Their description is complicated by the anisotropy of mechanical behavior in general and martensitic transformation in particular, the non-linearity of the material, hysteresis, tension-compression asymmetry and the temperature-dependence of the phenomena involved (Cisse et al., 2016; Machado & Lagoudas, 2008; Novák et al., 1999; Otsuka & Shimizu, 1986; Patoor et al., 1995; Peultier et al., 2006; Somerday et al., 1997). Some of the existing models do not take into account crystallographic orientation or grain interactions (Dimitris C. Lagoudas et al., 2006; Šittner & Novák, 2004). Other researchers introduce grain orientation through the use of the Schmid factor (*SF*) for stress induced martensitic transformation (*SIMT*) (Kaouache et al., 2006). A different approach was presented by (García-Castillo et al., 2015) where direct observation of the selected variants was made during a tensile test on polycrystalline martensite with known grain orientations. These authors proposed criteria based on the *SF* and on the strain tensor of the respective variants formed and concluded that the optimal criterion combines elements of both. However, this criterion has not been verified in single crystals.

This work analyses the crystallographic martensite variants (*MVs*) which are activated in a *Cu-Al-Be* monocrystal subject to a tensile test. The following theoretical aspects for the analysis were considered:

- The martensitic transformation is a thermoelastic diffusionless phase transformation, with first order phase transition, displacive and obtained by a shear deformation (Otsuka, K., &

Wayman, 1999; Bhadeshia H. K. D. K., 2014). Zhu (Zhu & Liew, 2003) and Balo (Balo et al., 2001) have described the martensitic transformation from *DO3* austenite (β phase) to *R18* martensite based on group theory and by using X-ray diffraction techniques. With the equations and data in both works it is possible to calculate and use by *Cu-Al-Be* the magnitude of shear (0.2324), the slip plane normal \mathbf{n} : [0.15, -0.65, 0.75] and the slip direction \mathbf{m} : [0.14, 0.73, 0.67] to obtain the 24 martensitic variants.

- Cortés (Cortés-Pérez, 2007) defined 3 reference systems, Figure 1., to develop a mathematical model simulating the distortion of the sample surface and to obtain the strain and displacement fields of a *SMA* undergoing the *SIMT* as a function of the crystalline orientation. With the observation base (\mathbf{e}_{0i}), canonic base (\mathbf{e}_i , associated to the crystal reference system) and transformation base ($\mathbf{e}_{i'}$) where $i = 1, 2, 3$. with coordinates $\mathbf{X}_0:(x_{10}, x_{20}, x_{30})$, $\mathbf{X}:(x_1, x_2, x_3)$ y $\mathbf{X}_i:(x_{1T}, x_{2T}, x_{3T})$.

The plots of *MVs* on the observation system can be obtained with equation 1. where \mathbf{n} is the normal to the habit plane in the canonic base, \mathbf{n}_0 the normal to the habit plane in the observation system and $A_{X \rightarrow X_0}$ is the matrix used to change the basis from transformation to observation system as a function of grain orientation. This matrix is the inverse of the matrix orientation \mathbf{g} and its possible calculate using the Euler angles ($\varphi_1, \phi, \varphi_2$) of the single crystal following Bunge convention (Bunge, 1982), equation 2.

$$\mathbf{n}_0 = A_{X \rightarrow X_0} \mathbf{n} \quad (1)$$

where:

$$A_{X \rightarrow X_0} = \mathbf{g}^{-1} \quad (2)$$

With \mathbf{g} is the direction cosine tensor of

system *X* in system X_0 .

- It is possible to use the Schmid Factor (*SF*) for the stress induced martensitic transformations (*SIMT*) because the martensitic variants formation is similar to dislocation slip on predetermined slip systems in conventional materials. This factor is defined by equation 3.

$$\tau_c^S = \sum_{ij} S_{ij} M_{ij}^S \quad (3)$$

Where τ_c^S is the critical resolved shear stress and M_{ij}^S , equation 4, is the Schmid tensor for the transformation system $n^\circ S$.

$$M_{ij}^S = \frac{1}{2} (\mathbf{m}_i^S \mathbf{n}_j^S + \mathbf{m}_i^S \mathbf{n}_j^S) \quad (4)$$

- The stress tensors are changed to the observation σ_{X_0} to transformation σ_{X_T} base knowing the matrix used to change the stress tensors for each reference systems defined by Cortés, equation 5.

$$\sigma_{X_T} = A_{X \rightarrow X_T} \cdot A_{X_0 \rightarrow X} \cdot \sigma_{X_0} \cdot A_{X \rightarrow X_0} \cdot A_{X_T \rightarrow X} \quad (5)$$

where:

$$\mathbf{g} = A_{X_0 \rightarrow X} \quad (6)$$

$$A_{X_T \rightarrow X} = \begin{pmatrix} m_1 & p_1 & n_1 \\ m_2 & p_2 & n_2 \\ m_3 & p_3 & n_3 \end{pmatrix} \quad (7)$$

$$\begin{pmatrix} p_1 \\ p_2 \\ p_3 \end{pmatrix} = \begin{pmatrix} m_1 \\ m_2 \\ m_3 \end{pmatrix} \times \begin{pmatrix} n_1 \\ n_2 \\ n_3 \end{pmatrix} \quad (8)$$

The matrix $A_{X_T \rightarrow X}$ is use to change the basis from transformation to canonic systems because the transformation systems are referred to the canonic basis.

- The plane stress transformational diagrams show the existence of specific variants according to the state of stress (in typical cases like: tension-tension, compression-tension, compression-compression and tension-compression), habit plane and

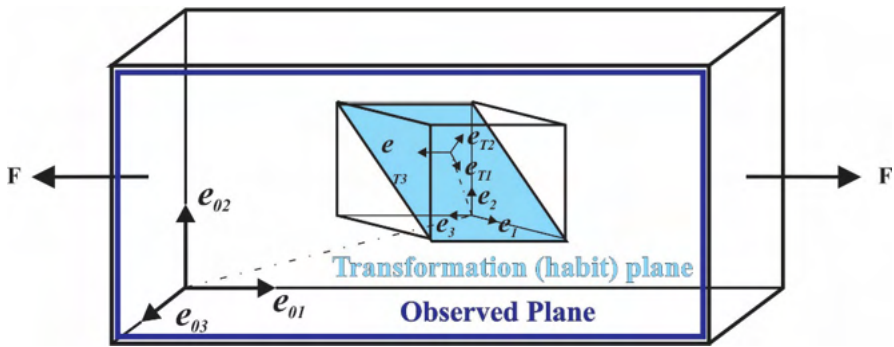


Figure 1. Reference systems used in the Cortés model.

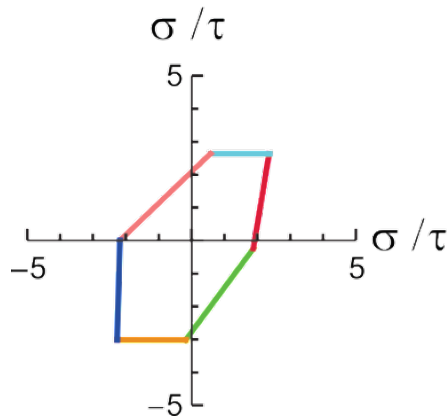


Figure 2. Example of a plane stress transformation diagram for a Cu-Al-Be alloy with an arbitrary crystallographic orientation. Each line in the diagram represents the activation of a specific martensite variant.

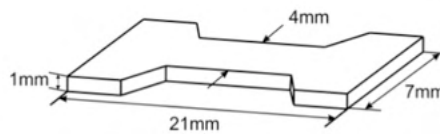


Figure 3. Tensile single crystal sample

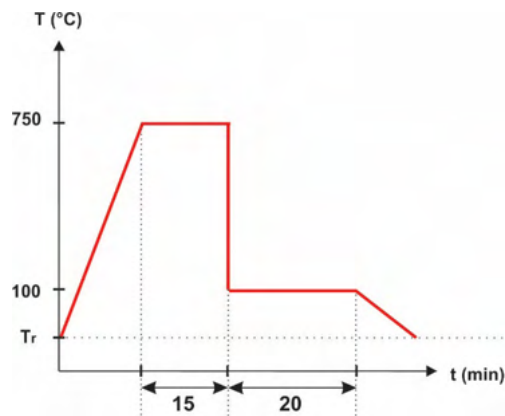


Figure 4. Heat treatment

crystal orientation. These diagrams were reported by (Buchheit et al., 1995; Buchheit & Wert, 1994; Comstock et al., 1996) Cu-Ni-Al and NiAl shape memory alloys (SMA for *Ni-Ti*, *Cu-Ni-Al*, *Ni-Al* and by (Martínez-Fuentes et al., 2013) for *Cu-Al-Be*. Figure 2.

EXPERIMENTAL

A single crystal sample of *Cu-Al-Be* was produced and donated by the Institut National des Sciences Appliquées (INSA), Lyon France. Its dimensions are shown in Figure 3.

The sample was beta-tized, to remove residual stress, according to the method of (Flores, 1993), following the annealing scheme shown in Figure 4.

The EBSD measurements performed to detect the crystalline orientation of the sample were performed in a scanning electron microscope, JEOL model JSM 6300, with INCA software. In this software, the crystallographic parameters of Cu-Al-Be must be introduced as follows: $DO3$ bcc, $a_0 = 5.82 \text{ \AA}$ and spatial group Fmm (225) (Balo et al., 2001; Tidu et al., 2001). The uniaxial tensile tests were conducted on a Deben-Gatan Microtest tensile device, which was coupled to an optical microscope from Leica MZ APO. The equipment included a load cell of 2 kN, and the strain rate of these tests was 0.2 mm/min.

The finite element analysis was realized using ABAQUS software. The linear anisotropic elastic constants for a *Cu-Al-Be* SMA as published by (Rios-Jara et al., 1991) were used for a cubic symmetry, with $C_{11} = 141.6 \text{ GPa}$, $C_{12} = 127.4 \text{ GPa}$, $C_{44} = 94.2 \text{ GPa}$. The reference systems defined in section 1 were defined in every ABAQUS simulation so that the crystallographic orientation for all elements was defined by the measured Euler angles $\varphi_1 = 181.6$, $\phi = 93.9$, $\varphi_2 = 345.4$.

RESULTS AND DISCUSSION

Figure 5. presents the martensitic variants formed by SIMT in the single crystal. In the central section, a single variant was formed (VM I) while on the fillet 3 variants are observed, one on the right side (VM II) and 2 in the left side (VM III and VM IV). For our analysis the 24 habit planes were plotted on the observation system using equation 1. In Figure 6. each variant is overlapped on the metallographic image at the sample center section. To facilitate the analysis, each variant is color coded.

The Schmid Factor was calculated for each martensite variant using equation 3. The maximum SF criteria was used to identify the variants formed. Table 1 provides the 4 expected martensite variants with the highest SF, shear stress and the variant number used by the authors.

A comparison between the MVs 8, 13, 20 and 18 with the real MVs shows a good coincidence. The selected MVs were within an angle deviation of less than 10° , considering a possible misalignment in the studied sample. The variant with maximum SF or maximum shear stress (MV8) is coincident with the MV observed at the sample center section, Table 2. This result validates the SF criterion as determined here for the single crystal case. Similarly, the remaining MVs 13, 20 and 18 were formed because the stress state is affected by the local geometry of the sample. Here as well, there is a good coincidence between the real MVs and the calculates, Table 2.

Figure 7. presents the plane stress transformational diagrams for the single crystal. The MVs 8 and 13 will appear if the state of stress is simple tension, tension-compression or low values in tension-tension. The MVs 20 and 18 will appear if the state of stress is simple tension or tension-tension.

Several MVs are showed in the plane stress transformation diagram, but some of them

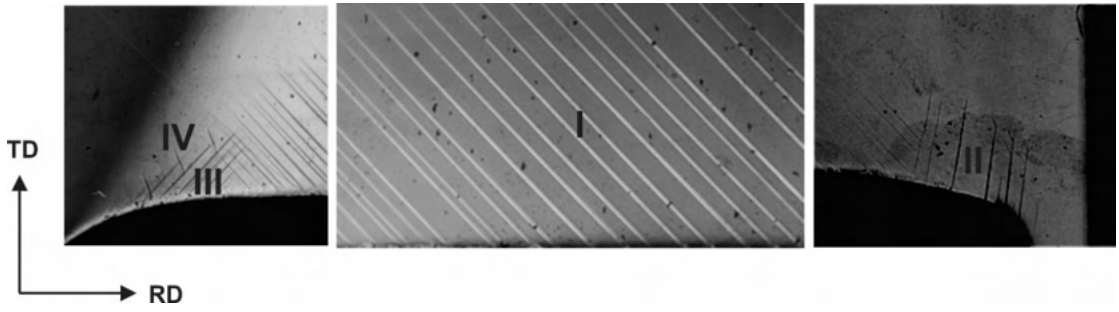


Figure 5. VMs formed by SIMT in the single crystal by SIMT.

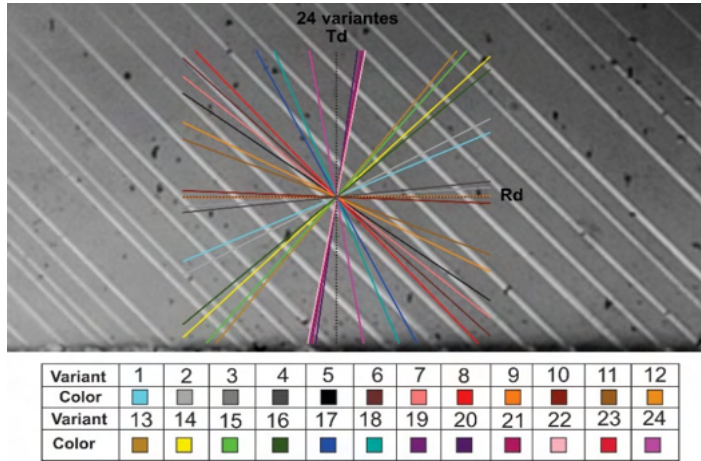


Figure 6. 24 possible martensitic variants overlapped on the microscopic image at the center of the single crystal sample.

Order	FS	f_{xy} (MPa)	VM
1	0.52	78.64	8
2	0.51	77.70	13
3	0.47	70.85	20
4	0.46	69.15	18

Table 1. 4 expected martensite variants with the highest SF and its martensitic variants.

Zone	Formed VM	τ_{xy} (MPa) uniaxial	τ_{xy} (MPa) FEM left	τ_{xy} (MPa) FEM right
Center	8	78.64	58.40	66.84
Left	13	77.70	79.10	64.74
	18	69.15	96.60	64.35
Right	20	70.85	66.86	66.86

Table 5. Comparison of maximum shear stress in MVs formed by region.

will never form because the single crystal is under tensile stress, for example the *MV24* or *MV4* will appear if the state of stress is compression and compression-compression. An element finite analysis was performed because the state of stress is unknown in the region of sample fillet. The simulations considered the crystallographic orientation and the cubic elastic constants for the single crystal. The stress distributions in the sample is showed in Figure 8, where the maximum values are at the fillets.

The regions of maximum stress coincide with the zones where the additional *MVs* were formed. The stress tensors in the elements with highest stress were extracted from *ABAQUS*, with γ representing the stress tensor at the left and right fillet in the observation basis. Differences between these tensors are expected because the crystal system axis is rotated with respect to the tensile axis. Using equation 5, both tensors were transformed to the canonic basis for all 24 *MVs*. Table 4 provides the 4 expected martensite variants with the highest shear stress and their variant number. The *MVs* formed in each size are in bold. The martensitic variants obtained by the stress tensors are the same that calculates with the *SF* criteria (8, 20, 13, 18) under pure tensile deformation, but in a different order, apart from *MV23* on the right fillet.

The highest shear stress over left side is the *MV18* and according to Table 2 it was formed. However, the next variant (23) was not formed; this result is compatible with the plane stress transformation diagram, Figure 7, because it is not a variant with minimal stress relation in contrast with the *MV13* which is very close to *MV8* with maximum *SF*. Another inconsistency is the *MV8* which does not appear in the list.

On the other hand, at the right side, the highest shear stress is the *MV20*, and it is formed. The next variant is the 8 with

similar value as the variant 20 (66.84 y 66.86 respectively). Table 5. presents a comparison between shear stress calculated assuming uniaxial tension and by *ABAQUS* simulations.

CONCLUSIONS

In this work, the *MVs* formed in a single crystal in a tensile test were compared with the calculated *MVs*. The calculations were based on the *SF* criterion for the state of the stress obtained by finite element simulation.

The following conclusions were found:

- a) The maximum *SF* criterion is consistent with the *SIMT* and validate the methodology used in this study. The variants with the highest shear stress were formed in the experiment.
- b) The variants on the plane stress transformational diagrams obtained for the single crystal are consistent with the real *MVs* formed.
- c) A *MV* with the highest shear stress was not formed. These inconsistencies may be due to considerations about finite element simulation because energy aspects were not used, or that the first variant formed reduces the stress in the region and prevents the formation of the second one.

ACKNOWLEDGMENTS

FNGC wishes to thank *DGAPA* for the post-doctoral fellowship in the project: “Interacción intergranular durante la transición elástico-plástico y la transformación martensítica incipiente en policristales: efectos de tamaño de grano y de memoria”. The authors thank the “instituto de tecnología de materiales” and “servicio de microscopia electrónica”, *UPV* Spain, for the crystallographic orientation measurement. Funding by grant *PAPIIT* IN115917 is acknowledged.

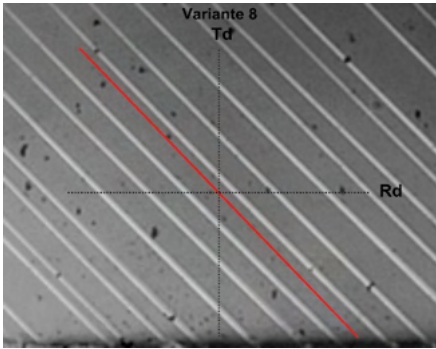
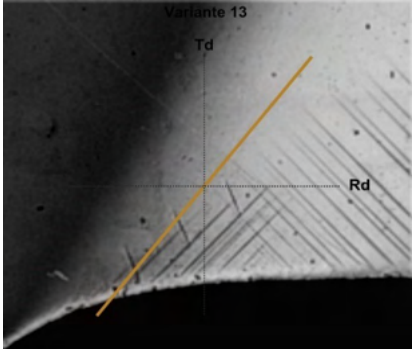
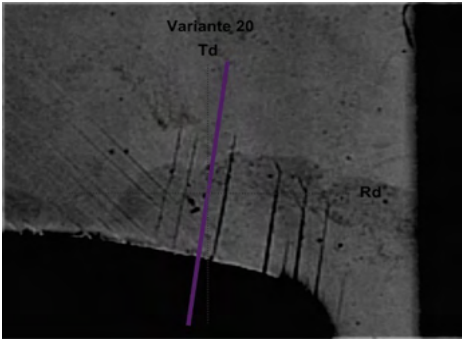
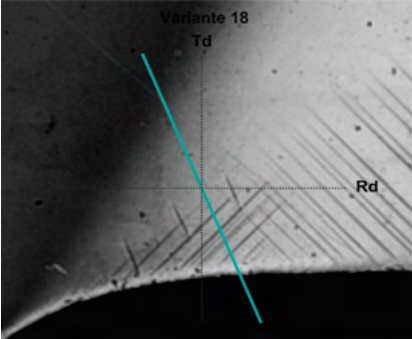
VM	Comparison	VM	Comparison
8		13	
20		18	

Table 2. *MV*'s with 4 highest *SF* overlapped on the several single crystal position.

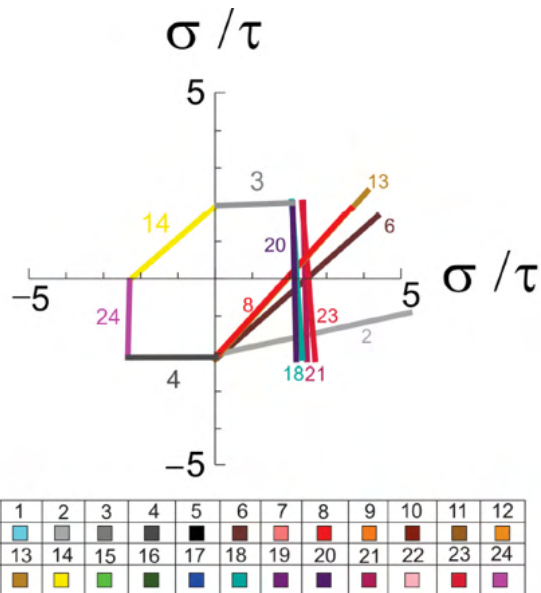


Figure 7. Plane stress transformation diagram for the single crystal studied here, accounting for the experimentally measured crystal orientation.

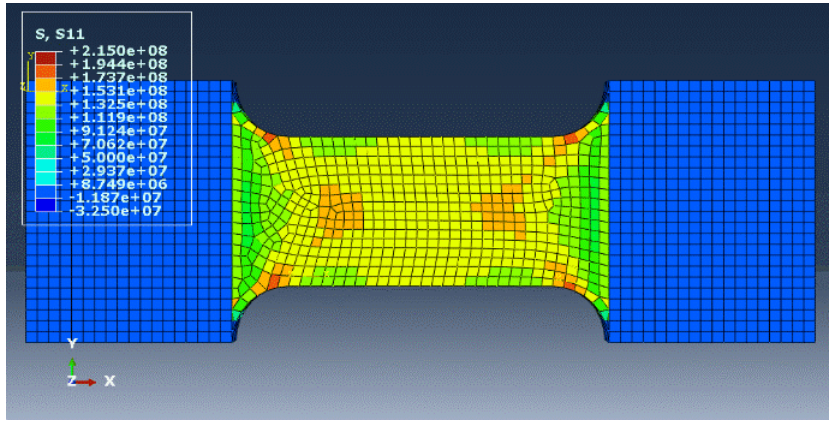


Figure 8. Simulation of stress distribution over sample in ABAQUS.

Size	Stress tensor
Left	$\sigma_{x_{0al}} = \begin{pmatrix} 174.29 \times 10^6 & 68.05 \times 10^6 & 10.73 \times 10^6 \\ 68.05 \times 10^6 & 44.74 \times 10^6 & 4.85 \times 10^6 \\ 10.73 \times 10^6 & 4.85 \times 10^6 & 4.24 \times 10^6 \end{pmatrix}$
Right	$\sigma_{x_{0ar}} = \begin{pmatrix} 143.46 \times 10^6 & -2.91 \times 10^6 & 1.59 \times 10^6 \\ -2.91 \times 10^6 & 10.16 \times 10^6 & 1.91 \times 10^6 \\ 1.59 \times 10^6 & 1.91 \times 10^6 & -604.78 \times 10^3 \end{pmatrix}$

Table 3. Stress tensor on the both regions with geometrical changes.

Size	τ_{xy} (MPa)	VM	Formed VM
	96.60	18	yes
Left	86.75	23	No
	79.10	13	yes
Right	71.46	20	No
	66.86	20	yes
	66.84	8	No
	64.74	13	No
	64.35	18	No

Table 4. Highest shear stress for state of stress obtained by ABAQUS on the transformation system.

REFERENCIAS

- Balo, S. N., Ceylan, M., & Aksoy, M. (2001). Effects of deformation on the microstructure of a Cu-Al-Be shape memory alloy. *Materials Science and Engineering A*, 311, 151–156.
- Bhadeshia H.K.D.K (2014). 9.5.6. Mechanical effects specific to thermoelastic transformations, in: *Physical Metallurgy, fifth edition*. © Elsevier B.V. All right reserved.
- Buchheit, T. E., Kumpf, S. L., & Wert, J. A. (1995). Modeling the stress-induced transformation behavior of shape memory alloy single crystals. *Acta Metallurgica Et Materialia*, 43(11), 4189–4199. [https://doi.org/10.1016/0956-7151\(95\)00105-5](https://doi.org/10.1016/0956-7151(95)00105-5)
- Buchheit, T. E., & Wert, J. A. (1994). Modeling the effects of stress state and crystal orientation on the stress-induced transformation of NiTi single crystals. *Metallurgical and Materials Transactions A*, 25(11). <https://doi.org/10.1007/BF02648858>
- Bunge, H.-J. (1982). Mathematical Aids. In *Texture Analysis in Materials Science* (pp. 351–403). <https://doi.org/10.1016/B978-0-408-10642-9.50019-2>
- Cisse, C., Zaki, W., & Ben Zineb, T. (2016). A review of constitutive models and modeling techniques for shape memory alloys. In *International Journal of Plasticity* (Vol. 76, pp. 244–284). <https://doi.org/10.1016/j.ijplas.2015.08.006>
- Comstock, R. J., Buchheit, T. E., Somerday, M., & Wert, J. A. (1996). Modeling the transformation stress of constrained shape memory alloy single crystals. *Acta Materialia*, 44(9), 3505–3514. [https://doi.org/10.1016/1359-6454\(96\)00014-6](https://doi.org/10.1016/1359-6454(96)00014-6)
- Cortés-Pérez, J. (2007). *Modelación matemática de la transformación martensítica inducida por esfuerzo*. Universidad Nacional Autónoma de México.
- Flores, H. (1993). *Estabilidad Térmica de la fase beta y del efecto memoria de forma doble de una aleación con memoria de forma tipo Cu-Al-Be*. Inst. Nat. Sc. Appl.
- Gao, X., Huang, M., & Brinson, L. C. (2000). Multivariant micromechanical model for SMAs. Part 1. Crystallographic issues for single crystal model. *International Journal of Plasticity*, 16(10), 1345–1369. [https://doi.org/10.1016/S0749-6419\(00\)00013-9](https://doi.org/10.1016/S0749-6419(00)00013-9)
- García-Castillo, F. N., Cortés-Pérez, J., Amigó, V., Sánchez-Arévalo, F. M., & Lara-Rodríguez, G. A. (2015). Development of a stress-induced martensitic transformation criterion for a Cu-Al-Be polycrystalline shape memory alloy undergoing uniaxial tension. *Acta Materialia*, 97, 131–145. <https://doi.org/10.1016/j.actamat.2015.06.044>
- Hall, G. J., Govindjee, S., Šittner, P., & Novák, V. (2007). Simulation of cubic to monoclinic-II transformations in a single crystal Cu-Al-Ni tube. *International Journal of Plasticity*, 23(1), 161–182. <https://doi.org/10.1016/j.ijplas.2006.04.004>
- Huang, M., & Brinson, L. C. (1998). A Multivariant model for single crystal shape memory alloy behavior. *Journal of the Mechanics and Physics of Solids*, 46(8), 1379–1409. [https://doi.org/10.1016/S0022-5096\(97\)00080-X](https://doi.org/10.1016/S0022-5096(97)00080-X)
- Kaouache, B., Inal, K., Berveiller, S., Eberhardt, A., & Patoor, E. (2006). Martensitic transformation criteria in Cu-Al-Be shape memory alloy-In situ analysis. *Materials Science and Engineering A*, 438–440(SPEC. ISS.), 773–778. <https://doi.org/10.1016/j.msea.2006.05.085>
- Kumar, P. K., & Lagoudas, D. C. (2008). Introduction to Shape Memory Alloys. In D. C. Lagoudas (Ed.), *Shape Memory Alloys* (pp. 29–40). Springer. <https://doi.org/10.1007/978-0-387-47685-8>
- Lagoudas, Dimitris C., Entchev, P. B., Popov, P., Patoor, E., Brinson, L. C., & Gao, X. (2006). Shape memory alloys, Part II: Modeling of polycrystals. *Mechanics of Materials*, 38(5–6), 430–462. <https://doi.org/10.1016/j.mechmat.2005.08.003>
- Lexcellent, C. (2013). Shape-memory Alloys Handbook. In *Shape-memory Alloys Handbook*. <https://doi.org/10.1002/9781118577776>

- Lu, Z. K., & Weng, G. J. (1998). A self-consistent model for the stress-strain behavior of shape-memory alloy polycrystals. *Acta Materialia*, 46(15), 5423–5433. [https://doi.org/http://dx.doi.org/10.1016/S1359-6454\(98\)00203-1](https://doi.org/http://dx.doi.org/10.1016/S1359-6454(98)00203-1)
- Machado, L. G., & Lagoudas, D. C. (2008). *Shape Memory Alloys* (Vol. 1). <https://doi.org/10.1007/978-0-387-47685-8>
- Martínez-Fuentes, R. J., Sánchez-Arévalo, F. M., Lara-Rodríguez, G. A., García-Castillo, F. N., Cortés-Pérez, F. M., & Reyes-Solís, A. (2013). Micromechanical Behavior of CuAlBe Shape Memory Alloy Undergoing 3-Point Bending Analyzed by Digital Image Correlation. In F. M. Braz Fernandes (Ed.), *Shape Memory Alloys - Processing, Characterization and Applications* (InTech). <https://doi.org/http://dx.doi.org/10.5772/48772>
- Novák, V., Šittner, P., Vokoun, D., & Zárubová, N. (1999). On the anisotropy of martensitic transformations in Cu-based alloys. *Materials Science and Engineering: A*, 273–275, 280–285. [https://doi.org/10.1016/S0921-5093\(99\)00355-X](https://doi.org/10.1016/S0921-5093(99)00355-X)
- Otsuka, K., & Wayman, C. M. (1999). Introduction. In C. M. Otsuka, K., & Wayman (Ed.), *Shape memory materials*. (pp. 1–25). Cambridge University Press.
- Otsuka, K., & Shimizu, K. (1986). Pseudoelasticity and shape memory effects in alloys. *International Metals Reviews*, 31(1), 93–114. <https://doi.org/10.1179/imtr.1986.31.1.93>
- Patoor, E., El Amrani, M., Eberhardt, a., & Berveiller, M. (1995). Determination of the Origin for the Dissymmetry Observed between Tensile and Compression Tests on Shape Memory Alloys. *Le Journal de Physique IV*, 05(C2), C2-495-C2-500. <https://doi.org/10.1051/jp4:1995276>
- Peultier, B., Ben Zineb, T., & Patoor, E. (2006). Macroscopic constitutive law of shape memory alloy thermomechanical behaviour. Application to structure computation by FEM. *Mechanics of Materials*, 38(5–6), 510–524. <https://doi.org/10.1016/j.mechmat.2005.05.026>
- Rios-Jara, D., Belkahlá, S., Canales, A., Flores, H., & Guénin, G. (1991). Elastic constants measurements of β Cu-Al-Be alloys. *Scripta Metallurgica et Materialia*, 25(6), 1351–1355. [https://doi.org/10.1016/0956-716X\(91\)90413-U](https://doi.org/10.1016/0956-716X(91)90413-U)
- Sánchez, F. M., & Pulos, G. (2006). Micro and Macromechanical Study of Stress-Induced Martensitic Transformation in a Cu-Al-Be Polycrystalline Shape Memory Alloy. *Materials Science Forum*, 509, 87–92. <https://doi.org/10.4028/www.scientific.net/MSF.509.87>
- Šittner, P., & Novák, V. (2004). Experiment feedbacks in micromechanics modeling of thermomechanical behaviors of SMA polycrystals. *Scripta Materialia*, 51(4), 321–326. <https://doi.org/10.1016/j.scriptamat.2004.04.022>
- Somerday, M., Comstock, R. J., & Wert, J. a. (1997). A systematic analysis of transformation stress anisotropy in shape memory alloys. *Philosophical Magazine A*, 75(5), 1193–1207. <https://doi.org/10.1080/01418619708209851>
- Tidu, A., Eberhardt, A., Bolle, B., Moreau, F., & Heizmann, J. (2001). *research papers Orthorhombic lattice deformation of CuAlBe shape- memory single crystals under cyclic strain research papers*. 1988, 722–729. <https://doi.org/10.1107/S002188980101384X>
- Yamauchi, K., Ohkata, I., Tsuchiya, K., & Miyazaki, S. (2011). *Shape memory and superelastic alloys*. Woodhead Publishing Limited. <https://doi.org/10.1533/9780857092625>
- Yoneyama, T., Miyazaki, S., Luo, H., Liao, Y., Abel, E., Wang, Z., & Liu, X. (2010). Shape memory alloys for biomedical applications. In *Shape Memory Alloys*. [https://doi.org/10.1016/S1369-7021\(08\)70257-8](https://doi.org/10.1016/S1369-7021(08)70257-8)
- Zamponi, C., Miranda, R. L. De, & Quandt, E. (2009). Superelastic thin films and applications for medical devices. In S. Miyazaki, Y. Q. Fu, & W. M. Huang (Eds.), *Thin Film Shape Memory Alloys-Fundamentals and Device Applications* (pp. 370–384). Cambridge University Press. <https://doi.org/https://doi.org/10.1557/mrs2002.43>
- Zhu, J. J., & Liew, K. M. (2003). Description of deformation in shape memory alloys from DO3 austenite to 18R martensite by group theory. *Acta Materialia*, 51(9), 2443–2456. [https://doi.org/10.1016/S1359-6454\(02\)00604-3](https://doi.org/10.1016/S1359-6454(02)00604-3)